



Canonical states in relativistic continuum theory with the Green's function method: Neutrons in continuum of zirconium giant-halo nuclei

X. Y. Qu (曲晓英)¹, H. Tong (童红)¹, and S. Q. Zhang (张双全)^{2,*}

¹*School of Mechatronics Engineering, Guizhou Minzu University, Guiyang 550025, China*

²*State Key Laboratory of Nuclear Physics and Technology, School of Physics, Peking University, Beijing 100871, China*



(Received 12 April 2021; accepted 23 December 2021; published 28 January 2022)

The canonical states in the relativistic continuum Hartree-Bogoliubov theory with Green's function method are obtained by diagonalizing the density matrix on a spatial mesh. Taking the giant halo nucleus ^{128}Zr as an example, the obtained canonical single-particle energies and wave functions are compared in detail with the corresponding calculations with the box-discretized method. The occupation number v_i^2 in the canonical basis and the neutrons in continuum N_c are investigated for the Zr giant halo nuclei. The dependencies on the pairing strength V_0 and on the different density functionals PK1 and NL-SH are also studied. It is found that the calculations with Green's function and box-discretized methods are almost consistent in describing nuclear global properties and the neutrons in continuum, meanwhile the N_c of giant halo nuclei may heavily depend on the adopted pairing strength as well as the density functional.

DOI: [10.1103/PhysRevC.105.014326](https://doi.org/10.1103/PhysRevC.105.014326)

I. INTRODUCTION

Since the discovery of halo structure in the 1980s by Tanihata *et al.* [1], numerous efforts have been undertaken to understand and explore this exotic phenomenon in nuclei far away from stability [2–10]. The first microscopic self-consistent interpretation to halo was provided in 1996 by Meng and Ring [11]. In their pioneering paper [11], by using the relativistic continuum Hartree-Bogoliubov (RCHB) theory [12], pairing correlations and the coupling to continuum states were revealed to play an essential role in the formation of halo. Later in 1998, they predict a more intriguing phenomenon named “giant halo” that contains a larger number of neutrons distributed in the halo [13].

So far, within the framework of the density functional theory (DFT) [14] or its covariant version (CDFT) [15], many investigations have been performed on the phenomena of halo [11,16–29] and giant halo [13,30–37]. To achieve a self-consistent description of halo nuclei with density functional theories, pairing correlations and suitable basis are two key points. For the former, treating the pairing correlations by the Bogoliubov transformation has turned out to be successful. For the latter, because of the extended spatial distribution of halo nuclei, it is appropriate to solving the (relativistic) Hartree-(Fock)-Bogoliubov equations in the coordinate space as in, e.g., Refs. [7,11–13,38–45], or in coordinate-like space [46–53]. In most of the DFT or CDFT studies of halo nuclei, however, the box boundary condition is adopted, so that the quasiparticle states are discretized and the exact asymptotic behaviors on the wave functions are missed for the weakly

bound and continuum states, which may have some influence on the studies of halo phenomena [37].

Green's function method [54] can provide the correct asymptotic behaviors on the wave functions, and has been combined with the DFT or CDFT calculations. Early in 1987, Belyaev *et al.* constructed the Green's function in the HFB theory in the coordinate representation [54]. Then Matsuo [55] applied it to calculate the response function in the quasiparticle random-phase approximation theory. To describe self-consistently both the mean field and the pairing potential, the fully self-consistent continuum Skyrme HFB theory with Green's function method was developed by Zhang *et al.* [37,56] and has been applied in Refs. [57–60]. On the CDFT side, the relativistic mean-field theory with the Green's function method was developed [61] and has been applied to describe the single-particle resonant states in atomic nuclei [62,63] and hypernuclei [64]. Meanwhile, the RCHB with Green's function method was also constructed to investigate the quasiparticle resonances and halo phenomena of the drip-line nuclei [65]. In addition, the Green's function method was also introduced in the complex scaling method [66,67], the complex momentum representation (CMR) method [68,69] as well as the coupled-channel representation [70] to study the resonant states.

In the Hartree-(Fock)-Bogoliubov theory, the canonical basis in which the density matrix is diagonal [71] plays an important role in understanding nuclear structure, such as showing shell structure evolution [12,38,44], discussing spin and pseudospin symmetries [72,73], studying continuum effects in weakly-bound and halo nuclei [11,13,37,56], and probing particles in classical forbidden regions [74]. Very recently, by diagonalizing the density matrix on a spatial mesh, the canonical states in the continuum Skyrme HFB theory with the Green's function were first obtained and

*sqzhang@pku.edu.cn

compared with those obtained by the box-discretized method by taking the exotic nucleus ^{66}Ca as an example [59]. It was demonstrated that the Green's function method can obtain the convergent canonical energy within a box size smaller than that of the box-discretized method, due to the correct asymptotic behaviors of the canonical wave functions. Following this line, it is interesting to obtain the canonical states in the framework of the RCHB with Green's function method.

In this paper, the canonical single-particle energy in RCHB theory with Green's function method is obtained by diagonalizing the density matrix in coordinate representation. Instead of ^{66}Ca discussed in Ref. [59], here we take the extreme neutron-rich Zr isotopes as examples, which are well known as a giant halo system [13] and have been extensively studied in nonrelativistic and relativistic density functional theories [32,33,35–37,75–77]. The obtained canonical single-particle energies and wave functions are compared in detail with the corresponding calculations with the box-discretized method. The occupation number v_i^2 in the canonical basis and the neutrons in continuum N_c are calculated for the Zr giant halo nuclei. In particular, we will study the dependencies on the pairing strength V_0 and on the different density functionals PK1 [78] and NL-SH [79] for the neutrons in continuum N_c .

II. THEORETICAL FRAMEWORK

The detailed formalism and numerical techniques of the RCHB theory can be found in Ref. [12], in which the box boundary condition was adopted. By using the Green's function method to provide the correct asymptotic behaviors of the wave functions, the RCHB with Green's function method was first developed in Ref. [65]. In this section, the corresponding formalism will be briefly introduced, followed by the process of obtaining the canonical states by diagonalizing the density matrix.

With the assumption of spherical symmetry, the RCHB equation depends only on the radial coordinates and is expressed as the following integral-differential equations [12]:

$$\begin{aligned}
& \frac{dG_U(r)}{dr} + \frac{\kappa}{r}G_U(r) - (E + \lambda - V(r) + S(r))F_U(r) \\
& + r \int r' dr' \Delta(r, r') F_V(r') = 0, \\
& \frac{dF_U(r)}{dr} - \frac{\kappa}{r}F_U(r) + (E + \lambda - V(r) - S(r))G_U(r) \\
& + r \int r' dr' \Delta(r, r') G_V(r') = 0, \\
& \frac{dG_V(r)}{dr} + \frac{\kappa}{r}G_V(r) + (E - \lambda + V(r) - S(r))F_V(r) \\
& + r \int r' dr' \Delta(r, r') F_U(r') = 0, \\
& \frac{dF_V(r)}{dr} - \frac{\kappa}{r}F_V(r) - (E - \lambda + V(r) + S(r))G_V(r) \\
& + r \int r' dr' \Delta(r, r') G_U(r') = 0,
\end{aligned} \tag{1}$$

in which $G_U(r)$, $F_U(r)$, $G_V(r)$, and $F_V(r)$ are respectively the large and small components of the radial wave functions for particle (ϕ_U) and hole (ϕ_V) parts, E the quasiparticle energy, λ the Fermi surface, $V(r)$ the vector potential, $S(r)$ the scalar potential with the nucleon mass M included, and $\Delta(r, r')$ the pairing potential. The quantum number κ is connected with the angular momentum quantum numbers l and j ,

$$\kappa = \begin{cases} -(j + 1/2), & \text{for } j = l + 1/2, \\ +(j + 1/2), & \text{for } j = l - 1/2. \end{cases} \tag{2}$$

The pairing potential Δ in Eq. (1) is

$$\Delta_{ab}(r, r') = V_{abcd}^{pp}(r, r') \kappa_{cd}(r, r'), \tag{3}$$

in which $V^{pp}(r, r')$ is the pairing interaction in the particle-particle channel and $\kappa(r, r')$ is the pairing tensor [71]. In practice, a density-dependent zero-range pairing force is adopted,

$$V^{pp}(r_1, r_2) = \frac{1}{2} V_0 (1 - P^\sigma) \delta(r_1 - r_2) \left(1 - \frac{\rho(r_1)}{\rho_{\text{sat}}} \right), \tag{4}$$

with V_0 the pairing strength, $\frac{1}{2}(1 - P^\sigma)$ the projector for the spin $S = 0$ component in the pairing channel, and ρ_{sat} the saturation density of nuclear matter.

Generally, one solves the RCHB equation (1) with box boundary condition and then the discretized eigenenergies and the corresponding quasiparticle wave functions are obtained. By summing over these discretized quasiparticle states, the density matrices ρ_s , ρ_v , ρ_3 , and ρ_c can be constructed [11–13,80],

$$\begin{aligned}
\rho_s(r, r') &= \frac{1}{4\pi r^2} \sum_{lj} [G_V^{lj*}(r) G_V^{lj}(r') - F_V^{lj*}(r) F_V^{lj}(r')], \\
\rho_v(r, r') &= \frac{1}{4\pi r^2} \sum_{lj} [G_V^{lj*}(r) G_V^{lj}(r') + F_V^{lj*}(r) F_V^{lj}(r')], \\
\rho_3(r, r') &= \frac{1}{4\pi r^2} \sum_{lj} \tau_3 [G_V^{lj*}(r) G_V^{lj}(r') + F_V^{lj*}(r) F_V^{lj}(r')], \\
\rho_c(r, r') &= \frac{1}{4\pi r^2} \sum_{lj} \frac{1}{2} (1 - \tau_3) [G_V^{lj*}(r) G_V^{lj}(r') \\
& + F_V^{lj*}(r) F_V^{lj}(r')],
\end{aligned} \tag{5}$$

which in turn determine the scalar and vector potentials in Eq. (1). In such way, the RCHB equations can be solved self-consistently.

The RCHB with Green's function method can provide the correct density asymptotic behavior and treat the bound and resonant states on the same footing [62]. By definition, the Green's function $\mathcal{G}(\mathbf{r}, \mathbf{r}'; E)$ describes the propagation of a particle with the energy E from \mathbf{r} to \mathbf{r}' . For a given quasiparticle energy E , the RCHB Green's function $\mathcal{G}(r, r'; E)$ obeys

$$[E - \hat{H}(r)] \mathcal{G}(r, r'; E) = \delta(r - r'). \tag{6}$$

It can be represented as

$$\mathcal{G}(r, r'; E) = \sum_k \left(\frac{\phi_k(r) \phi_k^\dagger(r')}{E - E_k} + \frac{\bar{\phi}_k(r) \bar{\phi}_k^\dagger(r')}{E + E_k} \right), \tag{7}$$

by using a complete set of eigenstates $\phi_k(r)$ and eigenvalues E_k of the RCHB equation [65]. Here $\phi_k(r)$ is the wave function corresponding to the positive energy solution E_k and $\bar{\phi}_k(r)$ the wave function corresponding to the negative energy solution $-E_k$.

In accordance to the four components $G_U(r)$, $F_U(r)$, $G_V(r)$, and $F_V(r)$ in the RCHB equation (1), the Green's function for the RCHB equation can be written in a form as a 4×4 matrix

$$\mathcal{G}(r, r'; E) = \begin{pmatrix} \mathcal{G}^{(11)} & \mathcal{G}^{(12)} & \mathcal{G}^{(13)} & \mathcal{G}^{(14)} \\ \mathcal{G}^{(21)} & \mathcal{G}^{(22)} & \mathcal{G}^{(23)} & \mathcal{G}^{(24)} \\ \mathcal{G}^{(31)} & \mathcal{G}^{(32)} & \mathcal{G}^{(33)} & \mathcal{G}^{(34)} \\ \mathcal{G}^{(41)} & \mathcal{G}^{(42)} & \mathcal{G}^{(43)} & \mathcal{G}^{(44)} \end{pmatrix}. \quad (8)$$

According to the Cauchy's theorem, the radial density matrices $\rho_{s,v}(r, r')$ and the pairing tensor $\kappa(r, r')$ can be calculated by the RCHB Green's function as [65]

$$\rho_s(r, r') = \frac{1}{2\pi i} \oint_{C_E > 0} dE [\mathcal{G}^{(33)}(r, r'; E) - \mathcal{G}^{(44)}(r, r'; E)], \quad (9a)$$

$$\rho_v(r, r') = \frac{1}{2\pi i} \oint_{C_E > 0} dE [\mathcal{G}^{(33)}(r, r'; E) + \mathcal{G}^{(44)}(r, r'; E)], \quad (9b)$$

$$\kappa(r, r') = \frac{1}{2\pi i} \oint_{C_E > 0} dE [\mathcal{G}^{(31)}(r, r'; E) + \mathcal{G}^{(24)}(r, r'; E)]. \quad (9c)$$

In practice, the RCHB Green's function $G_\kappa(r, r'; E)$ can be constructed with specific solutions satisfying the RCHB equation (1). Let us suppose $\phi_\kappa^{(rs)}(r, E)$ ($s = 1, 2$) to be the solutions of the RCHB equation (1) that satisfy the correct boundary condition at the origin $r = 0$, and $\phi_\kappa^{(+s)}(r, E)$ to be the solutions that satisfy the correct boundary condition at the edge of the box $r = R$. Here $s = 1, 2$ represent two independent solutions ϕ_U and ϕ_V , respectively. Then the RCHB Green's function can be given by [65]

$$\begin{aligned} G_\kappa(r, r'; E) = & \sum_{s, s'=1,2} c_\kappa^{ss'}(E) [\theta(r-r') \phi_\kappa^{(+s)}(r, E) \phi_\kappa^{(rs')\dagger}(r', E) \\ & + \theta(r'-r) \phi_\kappa^{(rs')}(r, E) \phi_\kappa^{(+s)\dagger}(r', E)]. \end{aligned} \quad (10)$$

The coefficients $c_\kappa^{(ss')}(E)$ are expressed in terms of the Wronskians as

$$\begin{pmatrix} c_\kappa^{11} & c_\kappa^{12} \\ c_\kappa^{21} & c_\kappa^{22} \end{pmatrix} = \begin{pmatrix} W_\kappa^{(r1,+1)} & W_\kappa^{(r1,+2)} \\ W_\kappa^{(r2,+1)} & W_\kappa^{(r2,+2)} \end{pmatrix}^{-1} \quad (11)$$

with

$$\begin{aligned} W_\kappa^{(rs,+s')} = & G_{u,\kappa}^{(rs)}(r, E) F_{u,\kappa}^{(+s')}(r, E) - G_{u,\kappa}^{(+s')}(r, E) F_{u,\kappa}^{(rs)}(r, E) \\ & - G_{v,\kappa}^{(rs)}(r, E) F_{v,\kappa}^{(+s')}(r, E) + G_{v,\kappa}^{(+s')}(r, E) F_{v,\kappa}^{(rs)}(r, E). \end{aligned} \quad (12)$$

Based on the RCHB Green's function thus constructed, one can calculate the radial density matrices and pairing tensor in Eqs. (9b) and (9c), and then solve the RCHB equations (1) by iteration.

In order to better understand the single-particle shell structure and analyze the contribution of the continuum to the exotic nuclei in the RCHB theory, the canonical single-particle basis and its occupation are useful. According to the Bloch-Messiah theorem [81], there always exists a so-called canonical basis in which the density matrix is diagonalized [71]. Here in RCHB, the canonical basis can be obtained by diagonalizing the radial density matrix, i.e., $\rho_v(r, r')$. This can be realized by solving the following integral eigenequation in the coordinate representation [82]:

$$\int dr' \rho_v(r, r') \Psi_k(r') = \Psi_k(r) v_k^2, \quad (13)$$

with v_k^2 the occupation numbers and $\Psi_k(r)$ the corresponding canonical wave functions. In the Green's function method, the density matrix $\rho_v(r, r')$ is given by Eq. (9b) and in the box-discretized method, given by Eq. (5). Similar to Ref. [83], the canonical single-particle energies can be calculated by the expectation values on the canonical basis of the Hamiltonian in the particle-hole channel h ,

$$\varepsilon_k = \langle \Psi_k | h | \Psi_k \rangle. \quad (14)$$

Furthermore, as mentioned in Ref. [59], if there exist nearly degeneracy states in the occupation number, it needs to diagonalize the Hamiltonian h in the subspaces constructed by those states with $v_k \approx 0$ or $v_k \approx 1$.

III. RESULTS AND DISCUSSION

A. Ground-state properties

In this paper, to study the canonical single particle states and the nucleons in continuum within the framework of the RCHB with Green's function, we focus on the very neutron-rich Zr nuclei. The covariant density functional PK1 [78] is adopted in the p-h channel, and the density dependent delta interaction (DDDI) is adopted in the p-p channel with the parameters $V_0 = -325.0 \text{ MeV fm}^3$ and the saturation density $\rho_0 = 0.152 \text{ fm}^{-3}$ in Eq. (4). In the calculations, the box size $R = 20 \text{ fm}$, the mesh size $\Delta r = 0.1 \text{ fm}$ and the angular momentum cut-off $j_{\text{cut}} = 19/2$ are adopted. The quasiparticle energy cut-off $E_{\text{cut}} = 110 \text{ MeV}$, the height $\gamma = 0.1 \text{ MeV}$ and the energy step $dE = 0.01 \text{ MeV}$ of the contour integration of the Green's function are chosen to reach the precision for $\rho(r)$ and $\kappa(r)$ up to 10^{-12} fm^{-3} and 10^{-8} fm^{-3} , respectively. It is noted that, due to the contour integral over each energy step, the RCHB with Green's function method needs about ten times more calculation time than the RCHB theory with the same box size. Similar ratio of computational time was obtained in the framework of Skyrme Hartree-Fock-Bogoliubov theory [59].

In Fig. 1, the ground-state properties, including the two-neutron separation energy S_{2n} , the neutron and proton root-mean-square (rms) radii r_{rms} , and the neutron and proton pairing energies E_{pair} , for the even-even Zr isotopes with mass number $A = 122$ to 140 obtained by the RCHB with Green's function method are shown, in comparison with those obtained by the RCHB theory.

The two-neutron separation energy S_{2n} provides a sensitive quantity to test a microscopic theory. As shown in Fig. 1(a),

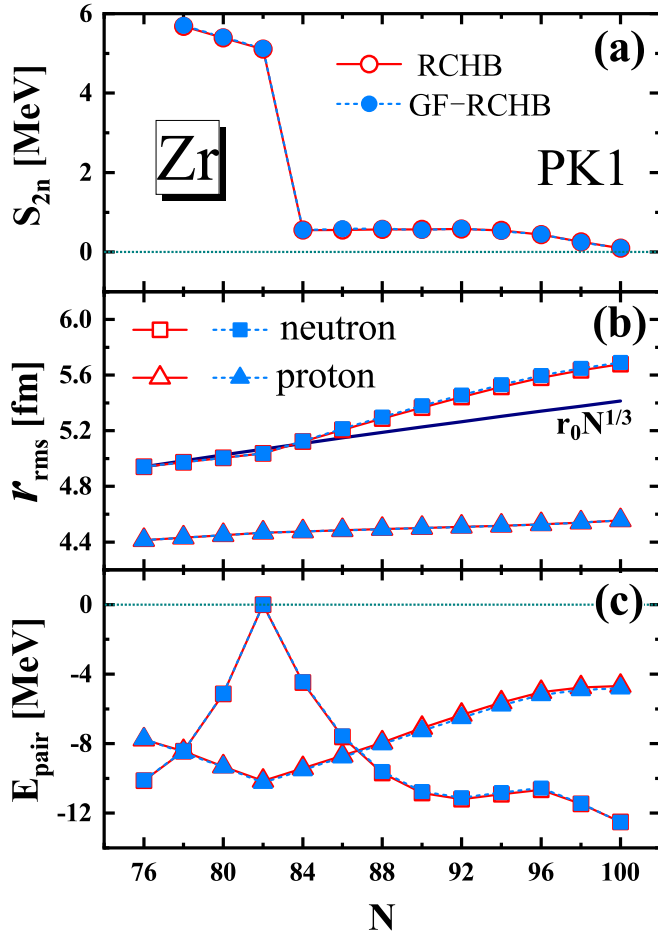


FIG. 1. Comparisons between (a) the two-neutron separation energies S_{2n} , (b) the neutron and proton rms radii r_{rms} , and (c) the neutron and proton pairing energies E_{pair} of the neutron rich Zr isotopes calculated by the RCHB with Green's function method (solid symbols) and those by the RCHB theory (open symbols). In both calculations, the density functional PK1 is adopted. In panel (b), the curve for the $r_0 N^{1/3}$ rule with $r_0 = 1.166$ fm has been included to guide the eye.

the S_{2n} values obtained by the two methods are consistent with each other. A strong drop in S_{2n} appears at the traditional magic number $N = 82$. Further addition of neutrons to the magic core puts the extra neutrons in the higher shell that provide few extra binding energies. As a result, the S_{2n} for $N > 82$ is less than 1 MeV and decreases slowly as the neutron number increases until nearly vanishing at $N = 100$ where the neutron drip line is reached. The drip line nucleus ^{140}Zr is the same as that predicted by the RCHB theory with the density functional NL-SH [13]. Similar to Refs. [13,31], the remarkable appearance of the S_{2n} values, i.e., extremely close to zero in several isotopes, indicates the existence of a "giant halo" in Zr isotopic chain.

In Fig. 1(b), the neutron and proton rms radii obtained by the two methods increases in similar way as the neutron number with each other. To guide the eye a curve with a $N^{1/3}$ dependence is also plotted. It shows a kink for the neutron rms radius at the magic neutron number $N = 82$, similar to

Ref. [13]. While the neutron rms radii before $N = 84$ follow the $r_0 N^{1/3}$ rule with $r_0 = 1.166$ fm, the radii after $N = 84$ show a more rapid increase with N . Examining the detailed values of the rms radii, it is found that the neutron rms radii obtained by the Green's function method are a little bit larger (differed by up to 0.3%) than those obtained by the discretized method. Both the proton rms radii increase slowly and monotonically by 0.14 fm from $N = 76$ to 100.

In addition to the physical observables S_{2n} and r_{rms} , it can be seen in Fig. 1(c) that the neutron and proton pairing energies obtained by the two methods are also consistent with each other. The neutron pairing energy vanishes at the closed shell $N = 82$ and the pairing effect appears a tendency of the enhancement when away from the magic nucleus ^{132}Zr . In contrast, the proton pairing energy reaches the minimum at the neutron magic number $N = 82$ and the pairing effect becomes weakened when away from ^{132}Zr .

Figure 1 shows the consistency between the Green's function and box-discretized methods in the description of the nuclear ground-state properties, a conclusion already obtained in Ref. [59] by comparing the two methods within the framework of Skyrme HFB. Here the conclusion is confirmed within the framework of relativistic Hartree-Bogoliubov theory.

B. Canonical states

To further analyze the formation of giant halos and figure out the continuum effects, the canonical single-particle states are very useful. In the RCHB theory, they can be obtained by diagonalizing the density matrix that constructed in the single-particle space [12]. In the RCHB with Green's function method, instead they are obtained by solving the integral eigenequation (13) for the density matrix. In the following, taking the nucleus ^{128}Zr as an example, the canonical single-particle energies and wave functions obtained in these two methods, in particular for the states in continuum, will be compared in detail.

Figure 2 shows the neutron canonical energies in continuum obtained by the RCHB with the Green's function method with the box size $R = 20$ fm. In comparison, the results obtained by the RCHB theory are also shown as functions of the box size R up to 30 fm. As shown in Fig. 2, energies of all the canonical states from the RCHB theory can converge with the increase of box size R , and the convergent results are consistent with those obtained by the Green's function method with $R = 20$ fm in a high accuracy. In detail, except the $4s_{1/2}$, $4p_{1/2}$, and $4p_{3/2}$ states with low orbital angular momentum l , all the canonical energies from the RCHB theory are almost independent on the box size for $R > 20$ fm. The three low- l states have low centrifugal barriers and relatively high canonical energies so that their wave functions would much disperse in space, as a consequence, they need a larger R to reach the convergence. Therefore, one can draw a similar conclusion to Ref. [59] that compared with the RCHB with box boundary condition, the convergent canonical energy can be achieved by the RCHB with Green's function method within a relatively smaller box size R .

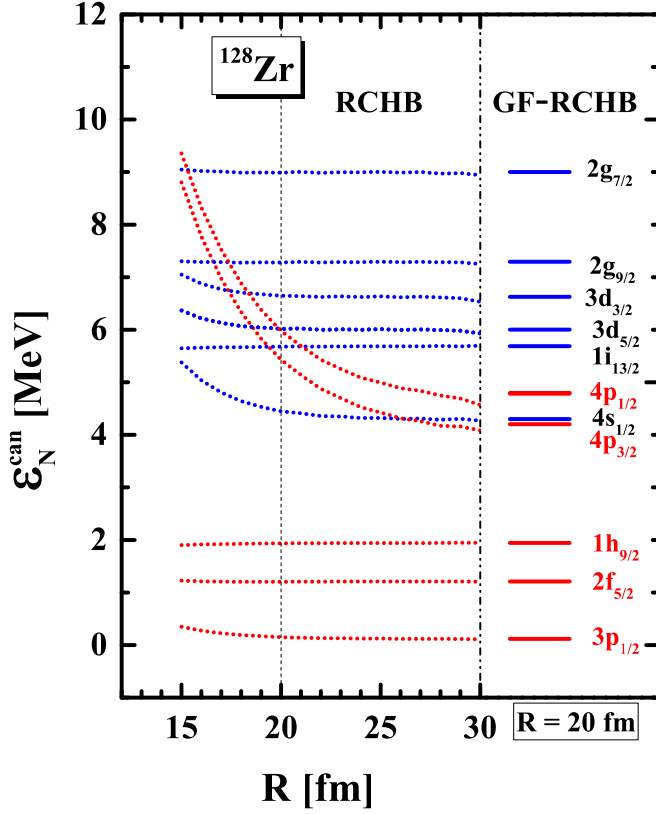


FIG. 2. Positive-energy canonical states in ^{128}Zr obtained by the Green's function method with the box size $R = 20$ fm (solid bars), in comparison with those obtained by the RCHB theory with different R (dash lines).

The wave functions $\Psi_i(r)$ of neutron canonical states $1p_{3/2}$, $3p_{3/2}$, $3p_{1/2}$, $2f_{5/2}$, $4p_{3/2}$, and $4s_{1/2}$ in ^{128}Zr obtained by the RCHB with Green's function method within different box sizes ($R = 15, 18,$ and 20 fm) are shown in Fig. 3, in comparison with those obtained by the RCHB theory. Among these states, the state $1p_{3/2}$ is deeply bound, the state $3p_{3/2}$ is extremely weakly bound, and the other four are states in continuum. It can be seen that the canonical wave functions of deeply bound state $1p_{3/2}$ obtained by the two methods are consistent with each other. In Figs. 3(a), 3(c), 3(e), 3(g), and 3(i), for these weakly bound and positive energy states, the canonical wave functions obtained by the Green's function method do follow the exponentially decreasing asymptotics and are independent on the box size. In contrast, as shown in Figs. 3(b), 3(d), 3(h), and 3(j), the canonical wave functions obtained by the RCHB theory decrease to zero at $R = 15, 18,$ and 20 fm, respectively, and in the near boundary regions depend on the box size. This is the consequence of the box boundary condition and the wave functions do not follow the exponentially decreasing asymptotics. This difference leads to the sensitive dependence of the corresponding canonical energy on the box size as given in Fig. 3. Note that for the state $2f_{5/2}$ with canonical energy $\varepsilon \approx 1.2$ MeV that has relatively high centrifugal barrier, the difference of canonical wave functions obtained by the RCHB theory is hardly seen in Fig. 3(f). Nevertheless, we can conclude that the RCHB with

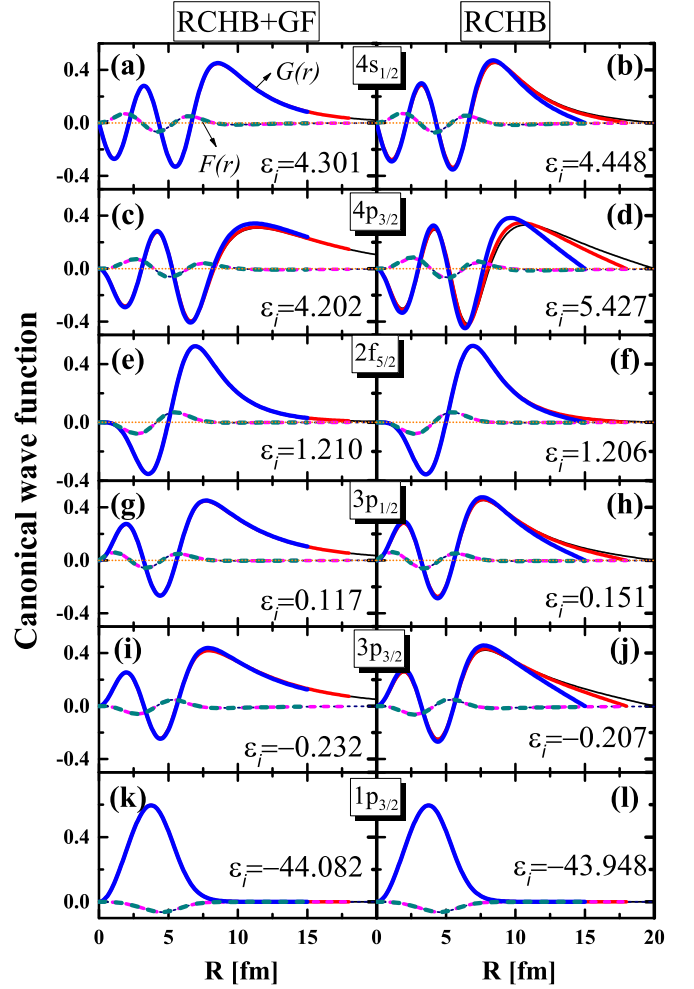


FIG. 3. Neutron canonical wave functions $\Psi_i(r)$ of $1p_{3/2}$, $3p_{3/2}$, $3p_{1/2}$, $2f_{5/2}$, $4p_{3/2}$, and $4s_{1/2}$ states for ^{128}Zr obtained by the Green's function [panels (a),(c),(e),(g),(i),(k)] and box-discretized [panels (b),(d),(f),(h),(j),(l)] method calculated with the box size $R = 15, 18,$ and 20 fm. The corresponding canonical single-particle energies ε_i calculated by Eq. (11) are also given in MeV.

the Green's function method provides more exact description of the canonical state with positive energies especially for the low- l levels.

C. Neutrons in continuum

In view of the advantage of the Green's function method, it is appropriate to further study the continuum effects in the halo nuclei by this method. Here taking different Zr isotopes as examples to exhibit the continuum effects, the neutron occupation probabilities v_i^2 of the canonical states for nuclei $^{124, 128, 132, 136}\text{Zr}$ as functions of the canonical single-particle energy in the interval $-20 \leq \varepsilon_i \leq 10$ MeV are shown in Fig. 4, together with their neutron density distributions in comparison with that of ^{122}Zr given in the inserts. To be more precise, those canonical single-particle states with a clear partial occupation ($0.01 < v_i^2 < 0.9$) are denoted by different symbols. The neutron Fermi surface λ_n is indicated by a vertical line and almost equals to zero in the neutron rich region.

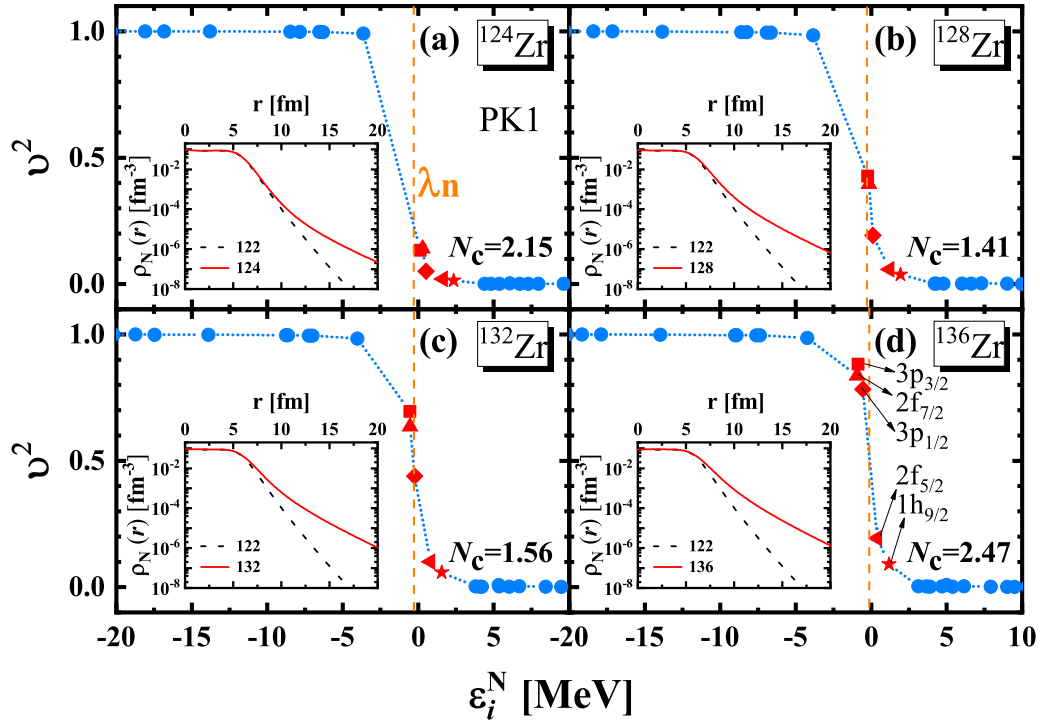


FIG. 4. The occupation probabilities in the canonical basis for nuclei $^{124,128,132,136}\text{Zr}$ as functions of the canonical single-particle energy. The Fermi surface λ_n is indicated by a vertical line. The number N_c of neutrons in continuum is also shown. The inserts give the neutron density of $^{124,128,132,136}\text{Zr}$ compared with the one of ^{122}Zr in logarithmic scale, respectively.

The nucleus ^{122}Zr has a magic neutron number and has no neutron pairing energy as shown in Fig. 1(c). By adding two neutrons to ^{122}Zr , the neutron pairing energy of ^{124}Zr becomes about -4.0 MeV. From Fig. 4(a), it can be seen that for the nucleus ^{124}Zr all the canonical single-particle states above the closure shell ($N = 82$) stay in continuum. Adding up the occupation probabilities v_i^2 for the states with $\varepsilon_i > 0$, we obtain the neutrons in continuum $N_c = 2.15$ for ^{124}Zr . The neutron density distribution of ^{124}Zr as shown in the insert becomes obviously diffuse in comparison with that of ^{122}Zr .

By adding more neutrons to ^{122}Zr , the neutron pairing energies of ^{128}Zr , ^{132}Zr , and ^{136}Zr become around -10 MeV. From Figs. 4(b)–(d), it can be seen for ^{128}Zr , ^{132}Zr , and ^{136}Zr there are significant increase in the occupation probabilities v_i^2 of the $3p_{3/2}$, $2f_{7/2}$, and $3p_{1/2}$ states, and the canonical energies of these states ε_i change from positive to negative, gradually below the Fermi surface. In addition, the occupation probabilities of higher canonical states $2f_{5/2}$ and $1h_{9/2}$ increase slowly, and their contributions to N_c also increase steadily from 0.35 and 0.37 for ^{128}Zr to 1.16 and 0.90 for ^{136}Zr . In total, the neutrons in continuum N_c obtained for ^{128}Zr , ^{132}Zr , and ^{136}Zr are 1.41, 1.56, and 2.47, respectively. As seen from the inserts, in comparison with the neutron density distributions of ^{122}Zr and even with that of ^{124}Zr , those of ^{128}Zr , ^{132}Zr , and ^{136}Zr become more diffuse in the asymptotic area as the neutron number increases, showing good examples of neutron halos for these nuclei.

If one compares the neutrons in continuum N_c of ^{124}Zr , ^{128}Zr , ^{132}Zr , and ^{136}Zr obtained here to those obtained in Ref. [13], some large differences between them can be found.

In the latter, the neutrons in continuum are two for ^{124}Zr , six for ^{128}Zr , roughly four for ^{132}Zr , and roughly four for ^{136}Zr [13]. In order to seek the reason of the differences of N_c , we take ^{128}Zr as an example and show the neutrons in continuum N_c obtained by the RCHB with Green's function method and the RCHB theory as functions of the pairing strength V_0 with density functionals PK1 and NL-SH, respectively. The results are given in Fig. 5. It can be seen that with either PK1 or NL-SH the N_c values from the two RCHB methods are very close to each other, which increase notably with the pairing

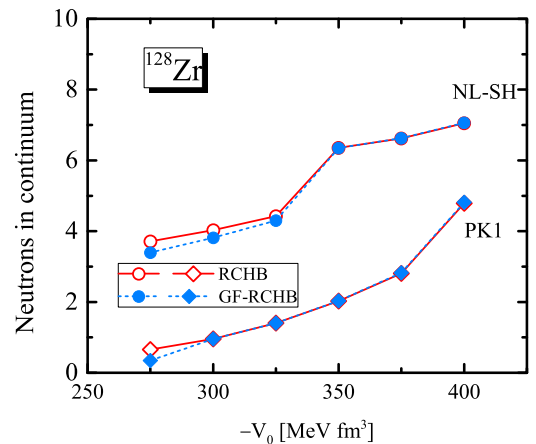


FIG. 5. Neutrons in continuum as functions of the pairing strength V_0 with parameters PK1 and NL-SH obtained by the RCHB with Green's function method and RCHB, respectively.

strength V_0 . But the N_c obtained with NL-SH does differ from the one with PK1 remarkably. For $V_0 = -350.0$ MeV fm³, one obtains N_c of ¹²⁸Zr is roughly six with NL-SH, whereas it is roughly two with PK1. Therefore, one can conclude that the number of neutrons in continuum in giant halo nuclei largely depends on the adopted density functional as well as the pairing strength. It is also noted in Fig. 5 that neutrons in continuum N_c obtained by usual RCHB theory is slightly higher than that by the RCHB with Green's function method. This behavior is not directly because of higher canonical single-particle energies with the RCHB theory compared to the RCHB with Green's function method (cf. Fig. 2), as a higher single-particle energy in continuum will lead to a smaller occupation number in continuum. However, it can be understood as an indirect consequence of higher canonical single-particle energies with the RCHB theory compared to the RCHB with Green's function method. That is, higher canonical single-particle energies of the low- l states in continuum with RCHB lead to their smaller occupation numbers; then conversely result in an increase of occupation numbers for high- l states; the self-consistent procedure of the theory tends to slightly lower canonical single-particle energies of the high- l states, until a delicate balance is reached.

IV. SUMMARY

The canonical states in the relativistic continuum Hartree-Bogoliubov theory with Green's function method are obtained by diagonalizing the density matrix on a spatial mesh. For the neutron-rich Zr nuclei, the ground-state properties including two-separation energy, rms radii and pairing energy, are calculated in comparison with those by discretized method. Taking the giant halo nucleus ¹²⁸Zr as an example, the obtained canonical single-particle energies and wave functions are compared as well. It is found that the calculations with

Green's function and box-discretized methods are almost consistent in describing nuclear global properties, but the former can provide more exact description of the canonical states with positive energies especially for the low- l levels. The occupation number v_i^2 in the canonical basis and the neutrons in continuum N_c are investigated for the Zr giant halo nuclei. The dependencies of N_c on the pairing strength V_0 and on the different density functionals PK1 and NL-SH are also studied for ¹²⁸Zr. It is found that the N_c values obtained by the Green's function and box-discretized methods agree with each other, although it may heavily depend on the adopted pairing strength and density functional. Finally, we note the present study is limited in the spherical case. It is very interesting to develop the deformed RCHB with the Green's function method to describe the deformed nuclei, and the technique presented in Ref. [70] may provide a way out for this purpose.

ACKNOWLEDGMENTS

The authors are indebted to J. Meng, K. Y. Zhang and Y. Zhang for the valuable suggestions during this work. This work was partly supported by the National Natural Science Foundation of China (Grants No. 11875075, No. 11935003, No. 11975031, No. 12070131001); the National Key R&D Program of China (Contracts No. 2017YFE0116700 and No. 2018YFA0404400); the State Key Laboratory of Nuclear Physics and Technology, Peking University (Grant No. NPT2020ZZ01); Youth Science and Technology Talent Project of Guizhou Province (No. KY[2021]105 and No. KY[2021]120); the Natural Science Research Project of Guizhou Minzu University (GZMUZK[2021]YB08); Science and Technology Foundation of Guizhou Province and Guizhou Minzu University (No. [2020]1Y027); Higher School Teaching Research Project (No. DJZW202039xn).

-
- [1] I. Tanihata, H. Hamagaki, O. Hashimoto, Y. Shida, N. Yoshikawa, K. Sugimoto, O. Yamakawa, T. Kobayashi, and N. Takahashi, *Phys. Rev. Lett.* **55**, 2676 (1985).
 - [2] I. Tanihata, *Prog. Part. Nucl. Phys.* **35**, 505 (1995).
 - [3] P. Ring, *Prog. Part. Nucl. Phys.* **37**, 193 (1996).
 - [4] B. Jonson, *Phys. Rep.* **389**, 1 (2004).
 - [5] A. S. Jensen, K. Riisager, D. V. Fedorov, and E. Garrido, *Rev. Mod. Phys.* **76**, 215 (2004).
 - [6] D. Vretenar, A. V. Afanasjev, G. A. Lalazissis, and P. Ring, *Phys. Rep.* **409**, 101 (2005).
 - [7] J. Meng, H. Toki, S.-G. Zhou, S. Q. Zhang, W. H. Long, and L. S. Geng, *Prog. Part. Nucl. Phys.* **57**, 470 (2006).
 - [8] T. Frederico, A. Delfino, L. Tomio, and M. T. Yamashita, *Prog. Part. Nucl. Phys.* **67**, 939 (2012).
 - [9] J. Meng and S.-G. Zhou, *J. Phys. G* **42**, 093101 (2015).
 - [10] Z. H. Yang, Y. Kubota, A. Corsi, K. Yoshida, X. X. Sun, J. G. Li, M. Kimura, N. Michel, K. Ogata, C. X. Yuan, Q. Yuan, G. Authalet, H. Baba, C. Caesar, D. Calvet, A. Delbart, M. Dozono, J. Feng, F. Flavigny, J.-M. Gheller *et al.*, *Phys. Rev. Lett.* **126**, 082501 (2021).
 - [11] J. Meng and P. Ring, *Phys. Rev. Lett.* **77**, 3963 (1996).
 - [12] J. Meng, *Nucl. Phys. A* **635**, 3 (1998).
 - [13] J. Meng and P. Ring, *Phys. Rev. Lett.* **80**, 460 (1998).
 - [14] I. Petkov and M. V. Stoitsov, *Nuclear Density Functional Theory* (Clarendon, Oxford, 1991).
 - [15] J. Meng, *Relativistic Density Functional for Nuclear Structure* (World Scientific, Singapore, 2016).
 - [16] W. Pöschl, D. Vretenar, G. A. Lalazissis, and P. Ring, *Phys. Rev. Lett.* **79**, 3841 (1997).
 - [17] G. Lalazissis, D. Vretenar, W. Pöschl, and P. Ring, *Nucl. Phys. A* **632**, 363 (1998).
 - [18] S. Mizutori, J. Dobaczewski, G. A. Lalazissis, W. Nazarewicz, and P. G. Reinhard, *Phys. Rev. C* **61**, 044326 (2000).
 - [19] S. Im and J. Meng, *Phys. Rev. C* **61**, 047302 (2000).
 - [20] J. Dobaczewski, W. Nazarewicz, and P. G. Reinhard, *Nucl. Phys. A* **693**, 361 (2001).
 - [21] V. Rotival and T. Duguet, *Phys. Rev. C* **79**, 054308 (2009).
 - [22] V. Rotival, K. Bennaceur, and T. Duguet, *Phys. Rev. C* **79**, 054309 (2009).
 - [23] S.-S. Zhang, E.-G. Zhao, and S.-G. Zhou, *Eur. Phys. J. A* **49**, 77 (2013).

- [24] S.-S. Zhang, M. S. Smith, Z.-S. Kang, and J. Zhao, *Phys. Lett. B* **730**, 30 (2014).
- [25] J. C. Pei, F. R. Xu, and P. Stevenson, *Nucl. Phys. A* **765**, 29 (2006).
- [26] J. C. Pei, Y. N. Zhang, and F. R. Xu, *Phys. Rev. C* **87**, 051302(R) (2013).
- [27] Y. J. Tian, Q. Liu, T. H. Heng, and J. Y. Guo, *Phys. Rev. C* **95**, 064329 (2017).
- [28] X. N. Cao, Q. Liu, and J. Y. Guo, *J. Phys. G* **45**, 085105 (2018).
- [29] X. N. Cao, Q. Liu, and J. Y. Guo, *Phys. Rev. C* **99**, 014309 (2019).
- [30] S. Q. Zhang, J. Meng, S.-G. Zhou, and J. Y. Zeng, *Chin. Phys. Lett.* **19**, 312 (2002).
- [31] J. Meng, H. Toki, J. Y. Zeng, S. Q. Zhang, and S.-G. Zhou, *Phys. Rev. C* **65**, 041302(R) (2002).
- [32] N. Sandulescu, L. S. Geng, H. Toki, and G. C. Hillhouse, *Phys. Rev. C* **68**, 054323 (2003).
- [33] S. Q. Zhang, J. Meng, and S.-G. Zhou, *Sci. China Ser. G* **33**, 289 (2003).
- [34] J. Terasaki, S. Q. Zhang, S.-G. Zhou, and J. Meng, *Phys. Rev. C* **74**, 054318 (2006).
- [35] M. Grasso, S. Yoshida, N. Sandulescu, and N. Van Giai, *Phys. Rev. C* **74**, 064317 (2006).
- [36] W. H. Long, P. Ring, J. Meng, N. Van Giai, and C. A. Bertulani, *Phys. Rev. C* **81**, 031302(R) (2010).
- [37] Y. Zhang, M. Matsuo, and J. Meng, *Phys. Rev. C* **86**, 054318 (2012).
- [38] J. Meng, I. Tanihata, and S. Yamaji, *Phys. Lett. B* **419**, 1 (1998).
- [39] J. Meng, K. Sugawara-Tanabe, S. Yamaji, P. Ring, and A. Arima, *Phys. Rev. C* **58**, R628 (1998).
- [40] J. Meng, S.-G. Zhou, and I. Tanihata, *Phys. Lett. B* **532**, 209 (2002).
- [41] H. F. Lv, J. Meng, S. Q. Zhang, and S.-G. Zhou, *Eur. Phys. J. A* **17**, 19 (2003).
- [42] W. Zhang, J. Meng, S. Q. Zhang, L. S. Geng, and H. Toki, *Nucl. Phys. A* **753**, 106 (2005).
- [43] W. H. Long, N. Van Giai, and J. Meng, *Phys. Lett. B* **640**, 150 (2006).
- [44] J. Dobaczewski, W. Nazarewicz, T. R. Werner, J. F. Berger, C. R. Chinn, and J. Dechargé, *Phys. Rev. C* **53**, 2809 (1996).
- [45] K. Bennaceur, J. Dobaczewski, and M. Ploszajczak, *Phys. Lett. B* **496**, 154 (2000).
- [46] M. V. Stoitsov, W. Nazarewicz, and S. Pittel, *Phys. Rev. C* **58**, 2092 (1998).
- [47] S.-G. Zhou, J. Meng, and P. Ring, *Phys. Rev. C* **68**, 034323 (2003).
- [48] S.-G. Zhou, J. Meng, P. Ring, and E.-G. Zhao, *Phys. Rev. C* **82**, 011301(R) (2010).
- [49] L. L. Li, J. Meng, P. Ring, E.-G. Zhao, and S.-G. Zhou, *Phys. Rev. C* **85**, 024312 (2012).
- [50] L.-L. Li, J. Meng, P. Ring, E.-G. Zhao, and S.-G. Zhou, *Chin. Phys. Lett.* **29**, 042101 (2012).
- [51] X.-X. Sun, J. Zhao, and S.-G. Zhou, *Phys. Lett. B* **785**, 530 (2018).
- [52] J. C. Pei, G. I. Fann, R. J. Harrison, W. Nazarewicz, Y. Shi, and S. Thornton, *Phys. Rev. C* **90**, 024317 (2014).
- [53] K. Zhang, M.-K. Cheoun, Y.-B. Choi, P. S. Chong, J. Dong, L. Geng, E. Ha, X. He, C. Heo, M. C. Ho, E. J. In, S. Kim, Y. Kim, C. H. Lee, J. Lee, Z. Li, T. Luo, J. Meng, M. H. Mun, Z. Niu *et al.*, *Phys. Rev. C* **102**, 024314 (2020).
- [54] S. T. Belyaev, A. V. Smirnov, S. V. Tolokonnikov, and S. A. Fayans, *Sov. J. Nucl. Phys.* **45**, 783 (1987).
- [55] M. Matsuo, *Nucl. Phys. A* **696**, 371 (2001).
- [56] Y. Zhang, M. Matsuo, and J. Meng, *Phys. Rev. C* **83**, 054301 (2011).
- [57] X. Y. Qu and Y. Zhang, *Sci. Chin. Phys. Mech. Astron.* **62**, 112012 (2019).
- [58] T. T. Sun, Z. X. Liu, L. Qian, B. Wang, and W. Zhang, *Phys. Rev. C* **99**, 054316 (2019).
- [59] X. Y. Qu and Y. Zhang, *Phys. Rev. C* **99**, 014314 (2019).
- [60] Y. Zhang and X. Y. Qu, *Phys. Rev. C* **102**, 054312 (2020).
- [61] T. T. Sun, S. Q. Zhang, Y. Zhang, J. N. Hu, and J. Meng, *Phys. Rev. C* **90**, 054321 (2014).
- [62] T. T. Sun, Z. M. Niu, and S. Q. Zhang, *J. Phys. G* **43**, 045107 (2016).
- [63] T.-T. Sun, W.-L. Lu, L. Qian, and Y.-X. Li, *Phys. Rev. C* **99**, 034310 (2019).
- [64] S. H. Ren, T. T. Sun, and W. Zhang, *Phys. Rev. C* **95**, 054318 (2017).
- [65] T. T. Sun, *Sci. Sin.-Phys. Mech. Astron. (in Chinese)* **46**, 012006 (2016).
- [66] M. Shi, J. Y. Guo, Q. Liu, Z. M. Niu, and T. H. Heng, *Phys. Rev. C* **92**, 054313 (2015).
- [67] M. Shi, X. X. Shi, Z. M. Niu, T. T. Sun, and J. Y. Guo, *Eur. Phys. J. A* **53**, 40 (2017).
- [68] Y. Shi, *Phys. Rev. C* **98**, 014329 (2018).
- [69] Y. Wang, Z. M. Niu, M. Shi, and J. Y. Guo, *J. Phys. G* **46**, 125103 (2019).
- [70] T. T. Sun, L. Qian, C. Chen, P. Ring, and Z. P. Li, *Phys. Rev. C* **101**, 014321 (2020).
- [71] P. Ring and P. Schuck, *The Nuclear Many-Body Problem* (Springer Science & Business Media, New York, 2004).
- [72] J. Meng, K. Sugawara-Tanabe, S. Yamaji, and A. Arima, *Phys. Rev. C* **59**, 154 (1999).
- [73] H. Z. Liang, J. Meng, and S.-G. Zhou, *Phys. Rep.* **570**, 1 (2015).
- [74] K. Y. Zhang, D. Y. Wang, and S. Q. Zhang, *Phys. Rev. C* **100**, 034312 (2019).
- [75] N. Schunck and J. L. Egido, *Phys. Rev. C* **78**, 064305 (2008).
- [76] S.-S. Zhang, X. D. Xu, and J. P. Peng, *Eur. Phys. J. A* **48**, 40 (2012).
- [77] K. M. Ding, M. Shi, J. Y. Guo, Z. M. Niu, and H. Z. Liang, *Phys. Rev. C* **98**, 014316 (2018).
- [78] W. H. Long, J. Meng, N. Van Giai, and S.-G. Zhou, *Phys. Rev. C* **69**, 034319 (2004).
- [79] M. M. Sharma, M. A. Nagarajan, and P. Ring, *Phys. Lett. B* **312**, 377 (1993).
- [80] W. Koepf and P. Ring, *Z. Phys. A* **339**, 81 (1991).
- [81] A. Messiah, *Quantum Mechanics* (North Holland, Amsterdam, 1962).
- [82] Y. Chen, P. Ring, and J. Meng, *Phys. Rev. C* **89**, 014312 (2014).
- [83] K. Bennaceur and J. Dobaczewski, *Comput. Phys. Comm.* **168**, 96 (2005).